Journal of Colloid and Interface Science 393 (2013) 80–86

Contents lists available at SciVerse ScienceDirect

Journal of Colloid and Interface Science

www.elsevier.com/locate/jcis

Stable photoluminescent $ZnO@Cd(OH)_2$ core–shell nanoparticles synthesized via ultrasonication-assisted sol–gel method

Jue-Fei Zhou, Jie Ao, Yong-Yao Xia, Huan-Ming Xiong *

Department of Chemistry and Shanghai Key Laboratory of Molecular Catalysis and Innovative Materials, Fudan University, 220 Handan Road, Shanghai 200433, PR China

ARTICLE INFO

Article history:
Received 28 July 2012
Accepted 25 October 2012
Available online 8 November 2012

Keywords:
ZnO
Core-shell nanoparticles
Ultrasonication
Photoluminescence

ABSTRACT

Core–shell structured $ZnO@Cd(OH)_2$ nanoparticles with stable and improved luminescence have been prepared successfully via a facile ultrasonication-assisted sol–gel method. Their composition and structure have been confirmed by high resolution transmission electron microscopy, X-ray diffraction, energy-dispersive X-ray spectroscopy, X-ray photoelectron spectroscopy, and infrared spectra. The size of the nanoparticles decreases gradually along with the increase in the shell thickness, indicating that $Cd(OH)_2$ shells can hider ZnO cores growth and aggregation effectively. The as-prepared core–shell nanoparticles can be stored at room temperature for several weeks without luminescence efficiency reduction, and they are quite stable at elevated temperatures or in moderate alkaline solutions due to the protection of the $Cd(OH)_2$ shell.

1. Introduction

Semiconductor nanoparticles (NPs), as a new class of luminescent materials, have shown potential applications in biological fluorescent labels [1,2], gas sensors [3,4], solar cells, and electronic transistors [5–8]. Among the well-known NPs, ZnO has the advantages of nontoxicity and cheapness, with a wide band gap (3.37 eV) and a large exciton binding energy (60 meV) at room temperature, and thus, ZnO NPs can be used in ultraviolet laser devices and biomedical labels [1,8]. However, ZnO NPs derived from the conventional sol–gel methods have relatively low quantum yield (QY) of visible emission due to the insufficient protection, and such prototypical ZnO NPs are usually not stable during storage [1,9,10]. Furthermore, their absorption spectra and fluorescence spectra exhibit gradual red-shift [11–33], because ZnO NPs tend to aggregate and undergo the Ostwald ripening process in colloids. ZnO visible emission originates from its defects which mainly locate on the surface of nanoparticles. Water is able to quench ZnO visible emission through surface passivation on oxygen vacancies [2]. Besides, many ions such as S^{2-}, $Fe^{2+/3+}$[34], Mn^{2+}[35–38], Co^{2+}[37] and Ni^{2+}[38,39], can also quench ZnO luminescence, which may be ascribed to the surface passivation effects or the trap of the photogenerated electrons on the ZnO surface. Shi et al. [33] reported that the unprotected ZnO colloids became turbid suspensions after only 2 or 3 days at room temperature. Therefore, sufficient surface protection is regarded as the key to obtain stable ZnO NPs with strong visible emission.

To improve ZnO stability various methods have been tried, including organic ligands modification, polymer capping, and inorganic shell coating. However, choosing a proper modification route faces challenges, especially that how to protect ZnO visible emission during chemical modification. Norberg and Gamelin [40] synthesized colloidal ZnO NPs capped by dodecylamine and trioctylphosphine oxide with uniform size and shape, but the ZnO green emission was very weak. Guo et al. [41] and Yang et al. [42] reported that ZnO NPs capped by poly(viny pyrrolidone) showed enhanced ultraviolet emission and dramatically reduced defect-related green emission. Inorganic shells, such as SiO_2[9], TiO_2[43], Al_2O_3[44,45], MgO [46] and $Zn(OH)_2$[47], were also employed for coating ZnO NPs. For instance, our group synthesized $ZnO@SiO_2$ core–shell NPs and such NPs were very stable in water, phosphate buffer saline, and cell culture medium [48]. But this inorganic-coating processes required multi-step complicated reactions which cost a lot of time [49,50]. Therefore, it is necessary to develop facile methods to synthesized ZnO nanoparticles with stable fluorescence in aqueous solutions.

Recently, significant progress in nanomaterial syntheses has been achieved by developing sonochemical techniques [51–54]. Upon irradiating liquids with ultrasound, the overgrowed bubbles will collapse and release the concentrated energy stored inside within a very short time (with a heating and cooling rate of over 10^{10} K s^{-1}). This cavitational implosion is very localized and transient with a temperature of 5000 K and a pressure of 1000 bar [46,55–58]. Cavitation-induced sonochemistry provides a unique interaction between energy and matter and permits access to the synthesis of a wide variety of unusual nanostructured materials. For example, we have successfully doped Mg^{2+} ions into ZnO NPs and the products exhibited strong and stable visible emission [59].

---

* Corresponding author. Fax: +86 21 55664397.
E-mail address: hmxiong@fudan.edu.cn (H.-M. Xiong).

0021-9797/$ - see front matter © 2012 Elsevier Inc. All rights reserved.
http://dx.doi.org/10.1016/j.jcis.2012.10.064

In this report, ZnO NPs were synthesized using a facile ultrasonication-assisted sol–gel route. The morphology and structure of the ZnO NPs were analyzed in detail using X-ray diffraction (XRD), transmission electron microscopy (TEM), X-ray photoelectron spectroscopy (XPS), and infrared spectra (IR). From these results, we believe the products were ZnO NPs coated by $Cd(OH)_2$, designated as $ZnO@Cd(OH)_2$ core–shell NPs. The UV–Vis absorption and photoluminescence measurements demonstrated that the QY of such $ZnO@Cd(OH)_2$ increased significantly as the Cd concentration increased. In the meantime, the stability of the $ZnO@Cd(OH)_2$ NPs was enhanced remarkably both at room temperature (for a month) and at elevated temperatures up to 90 °C, even in alkaline aqueous solutions.

2. Experimental

2.1. Materials

Dihydrated zinc acetate ($Zn(Ac)_2 \cdot 2H_2O$), monohydrated lithium hydroxide ($LiOH \cdot H_2O$), dihydrated cadmium acetate ($Cd(Ac)_2 \cdot 2H_2O$), and triethylene glycol (TEG) were all of analytical grade and purchased from Sinopharm Chemical Reagent Co., Ltd. Rhodamine 6G of high purity (Fluka) was used as a reference.

2.2. Synthesis of $ZnO@Cd(OH)_2$ NPs

0.878 g of $Zn(Ac)_2 \cdot 2H_2O$ and 0.252 g of $LiOH \cdot H_2O$ were mixed together in 80 ml of TEG at room temperature by stirring. After the solution became luminescent, different amount of $Cd(Ac)_2 \cdot 2H_2O$ was dissolved into the reaction system. Then, the solution was transferred into the ice-bath and sonicated by a titanium horn with a power of 1500 W for 30 min. To investigate the effect of Cd^{2+} ions on the optical properties of the core–shell nanoparticles, the synthetic molar ratios of Cd/Zn are adjusted from 0 to 0.8 (designated as x), and the Cd-free sample was used as the control. The as-prepared solutions were stored at room temperature.

2.3. Characterization

For UV–Vis absorption and photoluminescence (PL) measurements, a small amount of the as-prepared solution was extracted and diluted by absolute ethanol at different storage time. For XRD and XPS measurements, excess ethyl acetate was added into the as-prepared TEG solution to precipitate the white $ZnO@Cd(OH)_2$ gel. The gel was washed by ethyl acetate and centrifuged, followed by drying in a vacuum oven at 60 °C. PL spectra were recorded by a Varian Cary Eclipse fluorescence spectrophotometer. The UV–Vis absorption data were recorded by a Unico 2802PCS UV–Vis spectrometer. A Rhodamine 6G ethanol solution (QY = 95%) was used as the standard when evaluating the quantum yield of the colloids [2,10]. TEM images were obtained using a JEM-2100F field-emission transmission electron microscope operating at 200 kV with a point resolution of 0.20 nm. Element analysis was obtained by a XL30 scanning electron microscope with its energy-dispersive X-ray spectroscopy (EDS) in solid samples. To determine the Zn/Cd molar ratio in each sample, the powder was dissolved in an aqueous solution of HNO_3 via microwave digestion and measured by a Rayleigh WFX-110 inductively coupled plasma (ICP) mass spectrometer. XRD measurements were conducted on a Bruker D8 X-ray powder diffractometer. XPS analyses were carried out using a Perkin-Elmer PHI5000c. Infrared measurements were conducted on a Nicolet Impact 360 FTIR spectrometer. The average particle size was determined by dynamic light scattering using a Zetasizer Nano-ZS90 (Malvern Instruments).

3. Results and discussion

In XRD patterns of the $ZnO@Cd(OH)_2$ NPs and the control (Fig. 1), each peak corresponds to ZnO hexagonal phase of the wurtzite structure, and there are no signals of any other compounds. These ZnO diffraction peaks do not show any shift in comparison with the standard (JCPDS No: 79-0228), indicating that Cd^{2+} ions did not incorporate into the ZnO lattice. This result is in accord with the report by Mishra et al. [50] who proved their products were $ZnO@Cd(OH)_2$ core–shell NPs. The diffraction peaks of $Cd(OH)_2$ cannot be observed in the XRD patterns because the $Cd(OH)_2$ shells are thin and amorphous. As the Cd concentration increases, the XRD intensity of the $ZnO@Cd(OH)_2$ decreases and the full width at half maximum (FWHM) of the XRD peaks increases, indicating that ZnO cores become smaller and smaller. The average diameter (D) of ZnO NPs can be calculated by the Debye–Scherrer formula:

$$D = 0.89\lambda/\beta\cos\theta \tag{1}$$

where λ is the X-ray wavelength (K_α = 0.154184 nm), θ is the Bragg diffraction angle, and β is the FWHM of the XRD peak. After calculation, the mean sizes of the ZnO NPs are listed in Table 1, which vary from 4.1 nm to 2.8 nm along with adding Cd component.

The TEM images (Fig. 2) of the as-prepared samples show that the $ZnO@Cd(OH)_2$ NPs (x = 0.5) are uniform and monodispersed with an average diameter of about 2.8 nm, while the uncoated ZnO NPs have an average diameter of about 3.9 nm. Fig. 2D and E are HRTEM images of the $ZnO@Cd(OH)_2$ samples, in which the

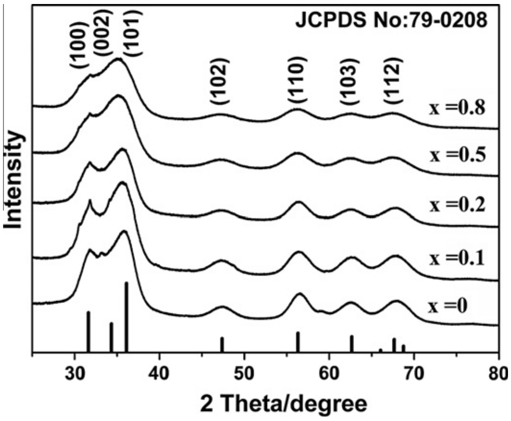

Fig. 1. XRD patterns of the as-prepared samples in solid powder.

Table 1
Comparison between the as-prepared nanoparticles with different Cd/Zn molar ratios (x).

x	ICP data[a]	Size[b] (nm)	Size[c] (nm)	Size[d] (nm)	Size[e] (nm)	Band gap[f] (eV)
0	0.000	3.9	8.7	4.1	3.9	3.45
0.1	0.066	3.5	10.1	3.8	3.7	3.49
0.2	0.099	3.3	14.6	3.6	3.4	3.55
0.5	0.405	2.9	16.9	2.9	2.9	3.64
0.8	0.550	2.8	19.6	2.8	2.7	3.68

[a] The actual Cd/Zn molar ratios were calculated from the ICP data.
[b] Statistics from the HRTEM images.
[c] Measured by DLS.
[d] Measured by XRD and evaluated by the Debye–Scherer formula.
[e] Measured by UV–Vis absorbance and calculated by Meulenkamp's empirical formula.
[f] Measured by UV–Vis absorbance and determined by the Tauc plot.

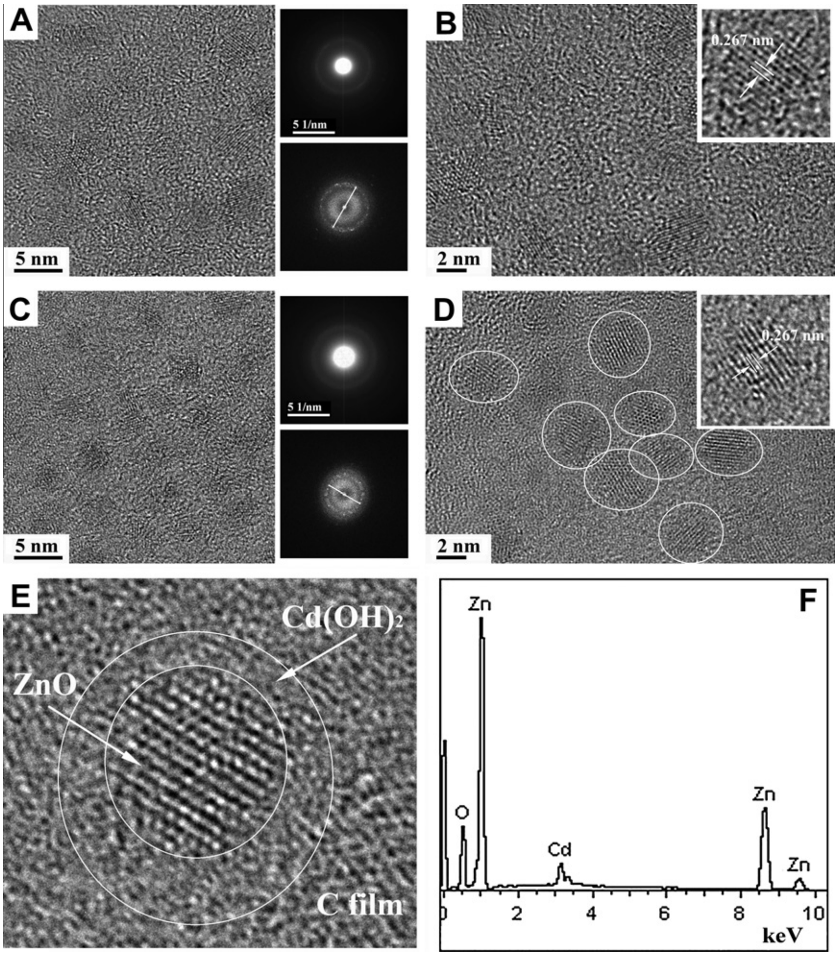

Fig. 2. HRTEM of the as-prepared (A, B) uncoated ZnO NPs and (C–E) core–shell ZnO@$Cd(OH)_2$ NPs. (F) EDS of the ZnO@$Cd(OH)_2$ powder obtained by SEM.

NPs are marked by white circles. In Fig. 2E, it can be seen that between the ordered ZnO lattice and the random black carbon dots of the carbon film on the copper meshes, there is a pale amorphous region, which is attributed to the amorphous shell of $Cd(OH)_2$. The HRTEM images and the Fast Fourier Transform (FFT) illustrate that both ZnO and ZnO@$Cd(OH)_2$ NPs have the same d-spacing value of 0.267 nm, which suggests that the Cd^{2+} ions did not incorporate into the ZnO lattice. The diffraction patterns of ZnO@$Cd(OH)_2$ NPs from the selected area electron diffraction (SAED, Fig. 2C inset) are vaguer than that of the uncoated ZnO, because the $Cd(OH)_2$ shells scattered the X-ray detection. The size of the as-prepared samples gradually reduces from 3.9 nm to 2.8 nm with the growth of the thickness of the $Cd(OH)_2$ shell. This phenomena can be explained by the competing reaction between $Zn(Ac)_2$ and $Cd(Ac)_2$ with LiOH. The $Cd(Ac)_2$ solution was added into the reaction system right after the ZnO NPs started to emit green luminescence. The hydrolysis reaction between $Cd(Ac)_2$ and LiOH under ultrasonic irradiation produced $Cd(OH)_2$ deposition on the ZnO surface and thus significantly inhibited the growth of ZnO NPs. The EDS spectrum by SEM (Fig. 2E) shows that zinc, cadmium, and oxygen are the main elemental components of the core–shell nanoparticles, which means cadmium exists in the form of $Cd(OH)_2$ or CdO rather than any other compounds. In general, $Cd(OH)_2$ decomposes and transforms into CdO above 250 °C. Hence, the cadmium compound produced from our preparation conditions can only be $Cd(OH)_2$. The actual Cd/Zn molar ratios in each sample obtained by ICP analyses were 0.000, 0.066, 0.099, 0.405, and 0.550 corresponding to $x = 0$, 0.1, 0.2, 0.5, and 0.8 (Table 1).

The hydrodynamic diameters of the samples in Fig. 3 reveal that the particle sizes have narrow distribution. Although the HRTEM and XRD results show that the ZnO diameter decreases when x value increases, the NP hydrodynamic size rises from 8.7 nm to 19.6 nm (Table 1) in the meantime because the DLS data include the thickness of the $Cd(OH)_2$ shells. More thicker the $Cd(OH)_2$ shells is, the more water molecules the NP adsorbs. And thus, the NP hydrodynamic sizes are much larger than the HRTEM and XRD results. Furthermore, the particle dispersion index (PDI) of the uncoated ZnO is 0.457, but the PDIs of the ZnO@$Cd(OH)_2$ NPs

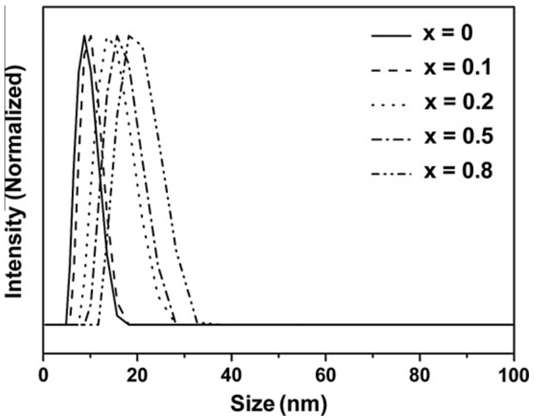

Fig. 3. DLS result of the as-prepared samples in water.

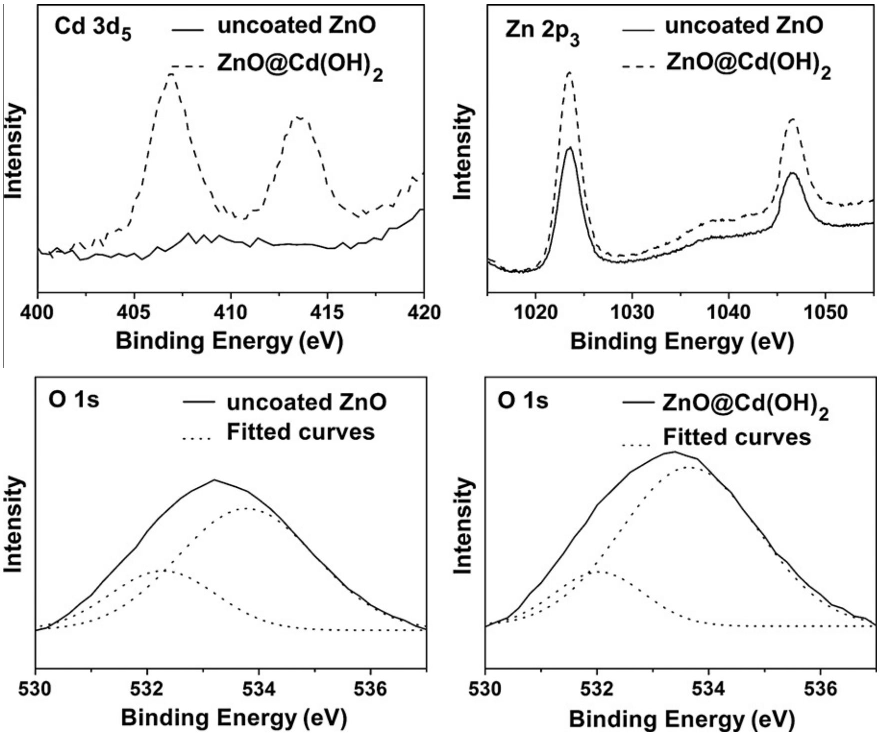

Fig. 4. XPS spectra of Cd $3d_5$, Zn $2p_3$, and O1s level for the uncoated and the $Cd(OH)_2$ capping ZnO.

are all close to 0.08. Hence, the core–shell NPs are nearly monodispersed in water while the uncoated ZnO NPs are not stable in water.

To confirm an effective Cd coating and its oxidation state on ZnO surface, XPS measurements were carried out. It can be seen from Fig. 4 that the Cd 3d region in ZnO@$Cd(OH)_2$ consists of the main $3d_{3/2}$ and $3d_{5/2}$ spin–orbit components at binding energies of 407 and 413 eV, respectively. These features are identical with other reported samples [60,61]. The high-resolution scan of Zn $2p_3$ level shows that after coating $Cd(OH)_2$ onto the ZnO surface, the peaks become narrow and slightly shift to the lower binding energy. According to the previous reports [62,13], decreasing ZnO nanoparticle size makes Zn 2p peak narrow. And the slight shift to the lower energy was attributed to the higher oxygen vacancy concentration in the smaller NPs [50,62]. The study on Zn $2p_3$ binding energy by Tay et al. [62] shows that the ZnO NP size reduction and the surface shrinkage render more oxygen vacancies and finally result in the narrower XPS peaks, and the peak shift toward the lower binding energy.

The asymmetric O1s peak corresponding to the uncoated ZnO NPs can be deconvoluted into two peaks centered at 532.3 and 533.8 eV, respectively, while those for the core–shell ZnO NPs located at 532.0 and 533.6 eV, respectively. The peak at the lower binding energy is ascribed to O atoms in ZnO wurtzite structure, and that of the higher binding energy can be attributed to oxygen atoms from the hydroxyl groups at NP surface. Comparing the uncoated and coated ZnO NPs, the O1s peak intensity at the lower binding energy are almost the same, but the O1s peak intensity at the higher binding energy of the ZnO@$Cd(OH)_2$ is significantly higher than that of the uncoated ZnO NPs, which proves that there are much more hydroxyl groups on the surface of the ZnO@$Cd(OH)_2$ NPs. In comparison with the report by Gulino et al. [60] (529.2 and 531.9 eV for the deconvoluted O1s peak), all of the O1s binding energy in our samples are relatively higher, indicating that our samples possess the higher concentrations of oxygen vacancies.

The IR spectra of the uncoated and the $Cd(OH)_2$-coating ZnO (Fig. 5) illustrate that the surface groups on both samples are similar. To identify the $Cd(OH)_2$ shell, the pure $Cd(OH)_2$ powder was also dried and measured by IR spectra. A sharp peak at 3607 cm^{-1} can be seen in the IR spectra, which is attributed to the free hydroxyl groups. However, for the nano-sized $Cd(OH)_2$ layer on ZnO surface, plenty of hydroxyl groups will not exist in a free form, but in complex association, which renders a broad IR band at about 3400 cm^{-1}. The Zn–O vibration band and the Cd–O vibration band are quite close, and they overlap each other in the IR spectra of the ZnO@$Cd(OH)_2$ sample, so that this sample exhibits enhanced absorption at around 470 cm^{-1}. In addition, the IR absorbance improvement for acetate groups coordinated on ZnO surface at 1416 and 1577 cm^{-1} in the ZnO@$Cd(OH)_2$ sample is ascribed to the larger surface area of the smaller ZnO cores [59].

The UV–Vis and PL spectra of the as-prepared samples are shown in Fig. 6. The UV–Vis absorbance onset blue-shifts when

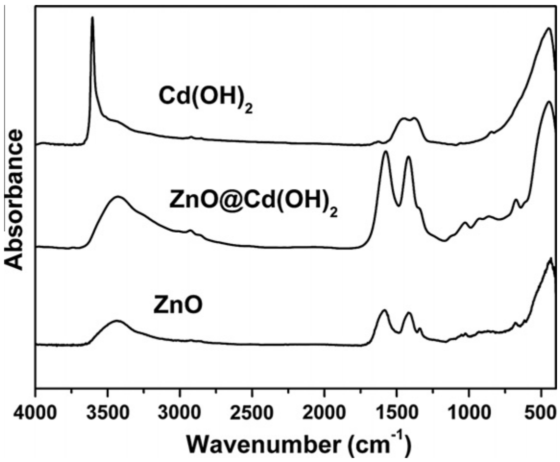

Fig. 5. FT-IR spectra of the samples in solid powder.

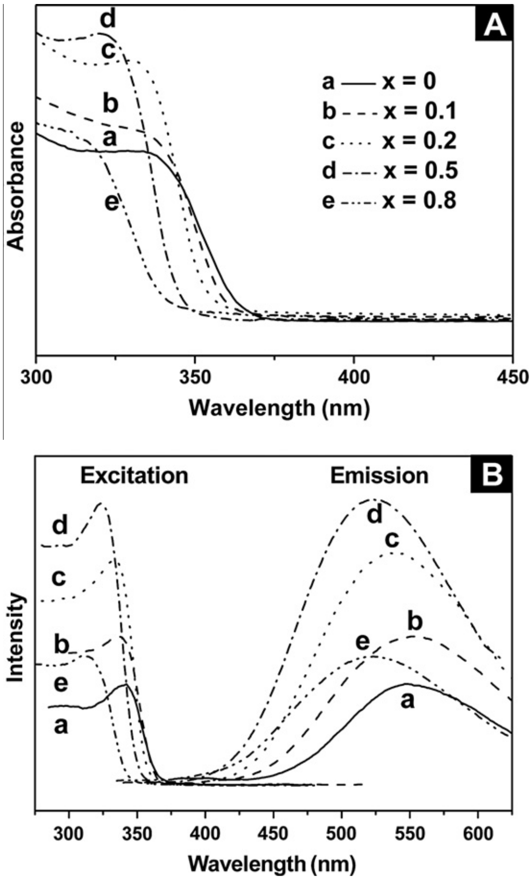

Fig. 6. (A) UV–Vis and (B) PL spectra of the as-prepared colloids.

the shell of $Cd(OH)_2$ thickens gradually, indicating that the average diameter of the ZnO cores reduces. If Cd^{2+} ions were doped into ZnO lattice, the absorbance onset should red-shift because CdO has a narrower band gap of 2.52 eV than ZnO (3.37 eV) [13]. This result reconfirms our speculation of the core–shell structure. From the UV–Vis data, the band gap values can be determined by the Tauc plot (Eq. (2)) and the corresponding ZnO diameters can be calculated using Meulenkamp's empirical formula (Eq. (3)).

$$(\alpha h\nu)^2 = A(h\nu - E_g) \tag{2}$$

$$1240/\lambda_{1/2} = a + b/D^2 - c/D \tag{3}$$

In Eq. (2), α equals to $-\ln T/d$ where T is the transmittance and d is the thickness of the quartz cuvette (1 cm), h is the Planck's constant, ν is the frequency of the photon, and E_g is the band gap energy [58]. To obtain the absorption onset, $(\alpha h\nu)^2$ was plotted versus energy $h\nu$ (called Tauc plot). The value of E_g was obtained by extending the Tauc plot until its intersection with $h\nu$ axis. In Eq. (3), $\lambda_{1/2}$ is the wavelength at which the absorption is half of that at the excitonic peak (or shoulder). When the ZnO diameter D is within the range 2.5–6.5 nm, a–c are parameters. The calculation results are listed in Table 1.

The photoluminescence spectra of the as-prepared samples exhibit broad green emission band in the visible region which is the typical ZnO defect emission. When the value of x increases, the PL intensity increases significantly till $x = 0.5$, and in the meantime, the maximum emission wavelength shows a slight blue shift, indicating the size reduction of the ZnO cores. When more $Cd(Ac)_2$ ($x > 0.5$) was added, ZnO NPs become smaller and the concentration of the obtained ZnO NPs decreases and the PL intensity drops quite a lot. The QY of these samples increases from 7.0% ($x = 0$) to 26.5% ($x = 0.5$), then decreases to 8.8% ($x = 0.8$), in accord with the trend of the PL intensity. The photoluminescence of ZnO NPs has two origins. One is the exciton emission which results from the recombination between photogenerated electrons and the holes at the valence band, while the other is defect-related emission in the visible region. Although the corresponding mechanisms of ZnO visible emission are complicated and have not been fully understood yet, numerous research reports have revealed that the surface oxygen vacancies play an important role in the luminescent process. The surface acetate groups have the advantage to maintain the oxygen vacancies, whereas some ligands like thiols and water are able to destroy the oxygen vacancies. Coating $Cd(OH)_2$ shell on the surface of ZnO NPs has shown the following merits. Firstly, the acetate groups on ZnO surface are well protected and the outside destructive molecules like water will be hindered. Secondly, the $Cd(OH)_2$ shell prevents the further growth and aggregation of ZnO NPs. Finally, according to van Dijken's study [20], the smaller fresh ZnO NPs possess the higher QY. Hence, the freshly formed ZnO NPs were coated by $Cd(OH)_2$ immediately, which maintained their optimal luminescent properties.

The comparison of the PL intensity evolution versus storage time under room temperature for the uncoated, and the core–shell structured ZnO have been illustrated in Fig. 7. Shi et al. [33] reported that the unmodified ZnO colloids became turbid suspensions after only 2 or 3 days, demonstrating that the uncoated ZnO NPs were not stable. For the ZnO@$Cd(OH)_2$ NPs in our research, the emission intensities are stable for 1 month at least. Interestingly, for the ZnO@$Cd(OH)_2$ mother colloids, the PL emission intensity kept enhancing at the initial stage of 10 days, suggesting that there remained unreacted $Zn(Ac)_2$ and LiOH after

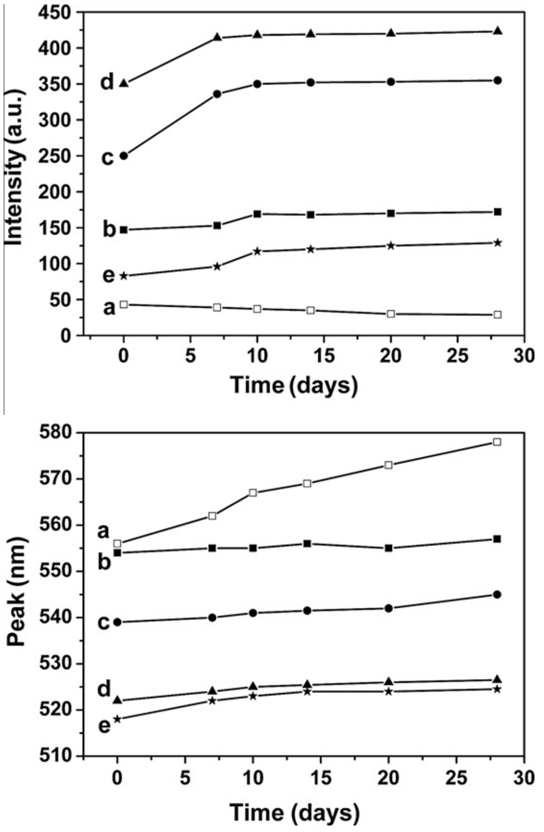

Fig. 7. The PL intensity and emission peak versus storage time under room temperature for the uncoated and the core–shell ZnO NPs. Sample a–e are synthesized by the different Cd/Zn molar ratios ($x = 0$, 0.1, 0.2, 0.5, and 0.8).

sonication which produced more ZnO NPs during storage. The competing reaction between the residual $Zn(Ac)_2$ and $Cd(Ac)_2$ continued until the ZnO NPs reached a new balanced concentration.

The thermostability of the ZnO@$Cd(OH)_2$ NPs has been investigated by heating scans (shown in Fig. 8). The PL intensity of the uncoated ZnO consecutively drops and the corresponding emission wavelength red-shifts as the temperature increases, which is typical for the growth and aggregation of ZnO NPs. In contrast, the PL spectra of the core–shell structured ZnO@$Cd(OH)_2$ NPs keep almost the same below 90 °C. Even when the solution temperature increases above 150 °C, in comparison with the uncoated ZnO, the $Cd(OH)_2$-coating ZnO NPs show much stronger fluorescence. Further research on the stability of the as-prepared samples in different buffer solutions has also been carried out (Fig. 9). The uncoated ZnO NPs were unstable in water and quickly turned turbid while the core–shell ZnO colloids kept clear. Particularly, the core–shell ZnO NPs are relatively more stable in alkaline solutions than in acidic solutions. In the latter condition, the $Cd(OH)_2$ shell was destroyed by acid and lost the capability of protection.

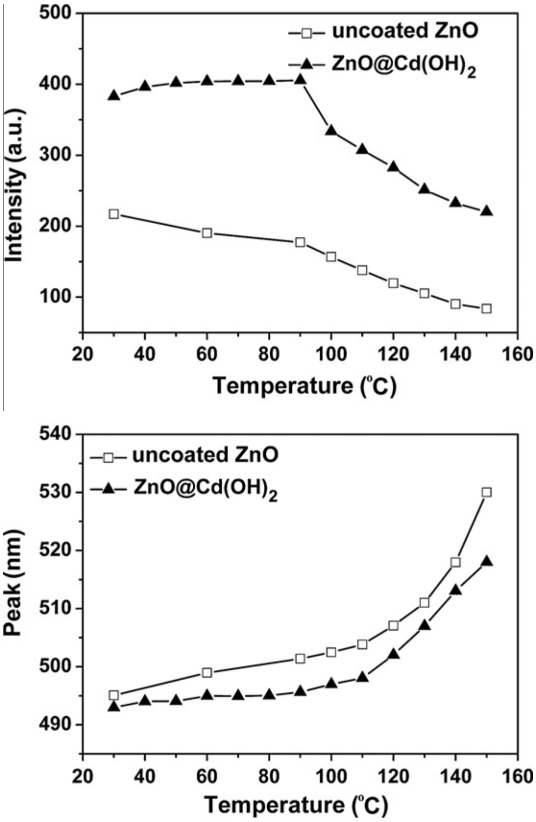

Fig. 8. The PL intensity changes and emission peak shifts during heating scans for the uncoated and the core–shell ZnO NPs.

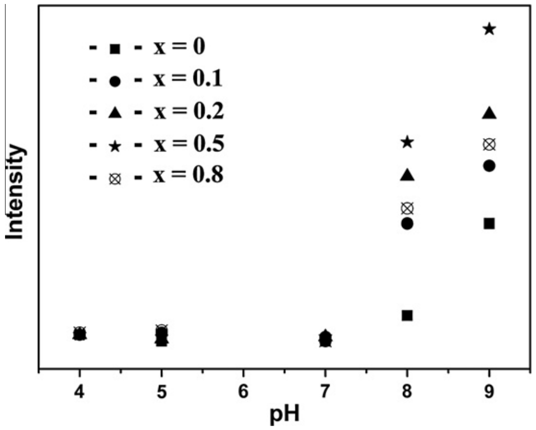

Fig. 9. The PL intensity of the emission maximum of the ZnO NPs prepared by different *x* in different pH buffer systems.

4. Conclusions

In summary, the core–shell ZnO@$Cd(OH)_2$ NPs with good stability and enhanced photoluminescence were successfully prepared via a facile ultrasonication-assisted sol–gel route. In the ultrasonic circumstance, acoustic cavitation creates extreme conditions inside the collapsing bubble and supplies a microenvironment for sonochemical reactions. $Cd(Ac)_2$ was hydrolyzed rapidly to form a thin protective shell of $Cd(OH)_2$ evenly deposited around the ZnO cores. Meanwhile, ultrasonic radiation lowers the viscosity of TEG solution and remarkably promotes the mass transport of materials via shock waves. Such conditions greatly shorten the reaction time that is usually needed for days. The $Cd(OH)_2$ shell protects the ZnO core from the outside destructive molecules and effectively prevents the further growth and aggregation of the ZnO NPs. The as-prepared ZnO@$Cd(OH)_2$ NPs are quite stable during storage at room temperature, as well as at elevated temperature and in the alkaline solutions. Our experiments suggest this ultrasonication-assisted sol–gel method as a rapid, simple, and effective way for the preparation of core–shell NPs.

Acknowledgments

This work was supported by the National Basic Research Program of China (2013CB934102), National Natural Science Foundation of China (Grant Nos. 20873029, and 21271045) and NCET-11-0115.

References

[1] P. Zhang, W.G. Liu, Biomaterials 31 (2010) 3087.
[2] H.M. Xiong, Y. Xu, Q.G. Ren, Y.Y. Xia, J. Am. Chem. Soc. 130 (2008) 7522.
[3] N.R. Jana, H.H. Yu, E.M. Ali, Y.G. Zheng, J.Y. Ying, Chem. Commun. 14 (2007) 1406.
[4] W.H. Zhang, W.D. Zhang, J.F. Zhou, J. Mater. Sci. 45 (2010) 209.
[5] Ü. Özgür, Ya.I. Alivov, C. Liu, A. Teke, M.A. Reshchikov, S. Do gan, V. Avrutin, S.J. Cho, H. Morkoc, J. Appl. Phys. 98 (2005) 041301.
[6] A.P. Alivisatos, Science 271 (1996) 933.
[7] Y. Yang, Y.Q. Li, S.Y. Fu, H.M. Xiao, J. Phys. Chem. C 112 (2008) 10553.
[8] L.P. Liu, J. Hensel, R.C. Fitzmorris, Y.D. Li, J.Z. Zhang, J. Phys. Chem. Lett. 1 (2010) 155.
[9] X.S. Tang, E.S.G. Choo, L. Li, J. Ding, J.M. Xue, Chem. Mater. 22 (2010) 3383.
[10] H.M. Xiong, D.P. Liu, Y.Y. Xia, J.S. Chen, Chem. Mater. 17 (2005) 3062.
[11] U. Koch, A. Fojtik, H. Weller, A. Henglein, Chem. Phys. Lett. 122 (1985) 507.
[12] D.W. Bahnemann, C. Kormann, M.R. Hoffmann, J. Phys. Chem. 91 (1987) 3789.
[13] M. Haase, H. Weller, A. Henglein, J. Phys. Chem. 92 (1988) 482.
[14] L. Spanhel, M. Anderson, J. Am. Chem. Soc. 113 (1991) 2826.
[15] M.S. Tokumoto, V. Briois, C.V. Santilli, S.H. Pulcinelli, J. Sol–Gel Sci. Technol. 26 (2003) 547.
[16] E.A. Meulenkamp, J. Phys. Chem. B. 102 (1998) 5566.
[17] P.D. Cozzoli, M.L. Curri, A. Agostiano, G. Leo, M. Lomascolo, J. Phys. Chem. B. 107 (2003) 4756.
[18] E.M. Wong, J.E. Bonevich, P.C. Searson, J. Phys. Chem. B. 102 (1998) 7770.
[19] E.A. Meulenkamp, J. Phys. Chem. B. 102 (1998) 7764.
[20] A. van Dijken, E.A. Meulenkamp, D. Vanmaekelbergh, A. Meijerink, J. Lumin. 90 (2000) 123.
[21] A. van Dijken, E.A. Meulenkamp, D. Vanmaekelbergh, A. Meijerink, J. Phys. Chem. B. 104 (2000) 1715.
[22] E.M. Wong, P.G. Hoertz, C.J. Liang, B.M. Shi, G.J. Meyer, P.C. Searson, Langmuir 17 (2001) 8362.
[23] Z. Hu, G. Oskam, P.C. Searson, J. Colloid Interface Sci. 263 (2003) 454.
[24] Z. Hu, G. Oskam, R.L. Penn, N. Pesika, P.C. Searson, J. Phys. Chem. B. 107 (2003) 3124.
[25] N.S. Pesika, K.J. Stebe, P.C. Searson, J. Phys. Chem. B. 107 (2003) 10412.

[26] A. Wood, M. Giersig, M. Hilgendorff, A. Vilas-Campos, L.M. Liz-Marzàn, P. Mulvaney, Aust. J. Chem. 56 (2003) 1051.
[27] H.Ch. Kuhn, R. Lipski, F. Seeler, D. Mauder, G. Müller, L. Spanhel, J. Sol–Gel Sci. Technol. 26 (2003) 499.
[28] Z.Y. Xiao, Y.C. Liu, L. Dong, C.L. Shao, J.Y. Zhang, Y.M. Lu, D.Z. Zhen, X.W. Fan, J. Colloid Interface Sci. 282 (2005) 403.
[29] L. Dong, Y.C. Liu, Y.H. Tong, Z.Y. Xiao, J.Y. Zhang, Y.M. Lu, D.Z. Shen, X.W. Fan, J. Colloid Interface Sci. 283 (2005) 380.
[30] H.M. Cheng, H.Ch. Hsu, S.L. Chen, W.T. Wu, Ch.Ch. Kao, L.J. Lin, W.F. Hsieh, J. Cryst. Growth 277 (2005) 192.
[31] Z. Zhu, T. Andelman, M. Yin, T.L. Chen, S.N. Ehrlich, S.P. O'Brien, R.M. Osgood, J. Mater. Res. 20 (2005) 1033.
[32] V. Noack, A. Eychm̈uller, Chem. Mater. 14 (2002) 1411.
[33] H.Q. Shi, W.N. Li, L.W. Sun, Y. Liu, H.M. Xiao, Sh.Y. Fu, Chem. Commun. 47 (2011) 11921.
[34] Y.S. Wang, P. John Thomas, P. O'Brien, J. Phys. Chem. B. 110 (2006) 21412.
[35] N.S. Norberg, K.R. Kittilstved, J.E. Amonette, R.K. Kukkadapu, D.A. Schwartz, D.R. Gamelin, J. Am. Chem. Soc. 126 (2004) 9387.
[36] R. Beaulac, P.I. Archer, D.R. Gamelin, J. Solid State Chem. 181 (2008) 1582.
[37] B. Panigrahy, M. Aslam, D. Bahadur, J. Phys. Chem. C. 114 (2010) 11758.
[38] W.W. Li, W.L. Yu, Y.J. Jiang, C.B. Jing, J.Y. Zhu, M. Zhu, Z.G. Hu, X.D. Tang, J.H. Chu, J. Phys. Chem. C. 114 (2010) 11951.
[39] C.H. Hung, W.T. Wang, J. Mater. Chem. 15 (2005) 267.
[40] N.S. Norberg, D.R. Gamelin, J. Phys. Chem. B. 109 (2005) 20810.
[41] L. Guo, S.H. Yang, C.L. Yang, P. Yu, J. Wang, G. Wong, Appl. Phys. Lett. 76 (2000) 2901.
[42] C.L. Yang, J.N. Wang, W.K. Ge, L. Guo, S.H. Yang, D.Z. Shen, J. Appl. Phys. 90 (2001) 4489.
[43] X.Q. Meng, H.W. Peng, Y.Q. Gai, J.B. Li, J. Phys. Chem. C. 114 (2010) 1467.
[44] J. Hwang, B. Min, J.S. Lee, K. Keem, K. Cho, M.Y. Sung, M.S. Lee, S. Kim, Adv. Mater. 16 (2004) 422.
[45] J.P. Richters, T. Voss, D.S. Kim, R. Scholz, M. Zacharias, Nanotechnology 19 (2008) 305202.
[46] D. Bera, L. Qian, P.H. Holloway, J. Phys. D: Appl. Phys. 41 (2008) 182002.
[47] H. Zhou, H. Alves, D.M. Hofmann, W. Kriegseis, B.K. Meyer, G. Kaczmarczyk, A. Hoffmann, Appl. Phys. Lett. 80 (2002) 210.
[48] H.J. Zhang, H.M. Xiong, Q.G. Ren, Y.Y. Xia, J.L. Kong, J. Mater. Chem. 22 (2012) 13159.
[49] H.M. Xiong, R.Z. Ma, S.F. Wang, Y.Y. Xia, J. Mater. Chem. 21 (2011) 3178.
[50] R. Mishra, R.S. Yadav, A.C. Pandey, S.S. Sanjay, Ch. Dar, J. Lumin. 130 (2010) 365.
[51] J.H. Bang, K.S. Suslick, Adv. Mater. 22 (2010) 1039.
[52] K.S. Suslick, S.B. Choe, A.A. Cichowlas, M.W. Grinstaff, Nature 353 (1991) 414.
[53] K.S. Suslick, Science 247 (1990) 1439.
[54] K.S. Suslick, Sci. Am. 260 (1989) 80.
[55] K.S. Suslick, D.J. Flannigan, Ann. Rev. Phys. Chem. 59 (2008) 659.
[56] A. Gedanken, Ultrason. Sonochem. 11 (2004) 47.
[57] M.A. Marguli, I.M. Margulis, High Energy Chem. 38 (2004) 285.
[58] D.G. Shchukin, E. Skorb, V. Belova, H. Möhwald, Adv. Mater. 23 (2011) 1922.
[59] H.M. Xiong, D.G. Shchukin, H. Möwald, Y. Xu, Y.Y. Xia, Angew. Chem. 121 (2009) 2765.
[60] A. Gulino, P. Dapporto, P. Rossi, I. Fragala, Chem. Mater. 14 (2002) 1441.
[61] N. Singh, S. Charan, K.R. Patil, A.K. Viswanath, P.K. Khanna, Mater. Lett. 60 (2006) 3492.
[62] Y.Y. Tay, S. Li, C.Q. Sun, P. Chen, Appl. Phys. Lett. 88 (2006) 173118.